Schrödinger equation description for cross-phase modulation in grating structures

M. J. Steel and C. Martijn de Sterke
School of Physics and Optical Fibre Technology Centre, University of Sydney, New South Wales 2006, Australia
(Received 28 October 1993)

We present a simple approximate description of systems involving cross-phase modulation in highly dispersive media. Optical pulses in such systems suffer large frequency shifts and correspondingly experience large variations in group velocity dispersion so that a simple nonlinear Schrödinger equation description is not valid. We take the frequency shift into account in a moments based model that extends the standard Schrödinger description, and apply the model to the particular case of optical pulse compression in nonlinear Bragg gratings. The model is tested against full numerical simulations. Finally, we consider some of the difficulties involved in observing the pulse-compression effect.

PACS number(s): 42.65.Re, 42.65.Vh

I. INTRODUCTION

The nonlinear Schrödinger equation (NLSE) and systems of coupled nonlinear Schrödinger equations have become the generic models for much of nonlinear guided wave optics. Predictions of the NLSE for standard optical fibers have been strikingly confirmed experimentally, most notably in the observation of optical-fiber solitons [1]. Processes such as pulse compression via cross-phase modulation have been described accurately by coupled nonlinear Schrödinger equations [2]. The NLSE has also been applied to nonlinear wave propagation in periodic media [3,4]. Here we wish to examine a case where a nonlinear Schrödinger-like equation is not valid without extension, namely, that of induced frequency shifts in periodic media, or more generally, in media where the group velocity and dispersion are rapidly varying functions of frequency.

Gratings, or periodic structures, are media in which the dielectric constant is a periodic function of distance. The linear dispersion relation around the Bragg resonance for such a grating is shown in Fig. 1, superimposed with the dispersion relation for a uniform medium. The presence of the grating produces a photonic band gap centered at the Bragg frequency $\omega_0 = \pi c/(nd)$, where n is the average refractive index of the grating which has period d. In the linear regime, frequencies lying inside the band gap are strongly coupled to modes traveling in the opposite direction and do not propagate through the medium. Frequencies outside the band gap propagate with group velocities given by the slope of the dispersion relation, and experience group-velocity dispersion given by the curvature of the dispersion relation. Thus waves which are strongly detuned from the Bragg resonance (e.g., the plus in Fig. 1) propagate virtually unimpeded: they travel with the velocity c/n of light in a uniform medium of the same average refractive index, and see a small dispersion. Close to the Bragg resonance (e.g., circle in Fig. 1), however, the group velocity varies between 0 and c/n, and the dispersion increases to a maximum at the band edge.

Grating structures can be fabricated in a range of materials including semiconductor waveguides [5], thin-film stacks, and optical fibers [6]. In the numerical work to follow, we consider a waveguide structure made from alternating layers of GaAs and $Al_xGa_{1-x}As$. For such a device, index variations can easily reach $\Delta n = 0.1$. For our examples we take a weaker grating with $\Delta n = 0.042$ and mean index $n = 3.14$. With this value, the band gap has a width of $\Delta f = \kappa c/(n\pi) = 2.44 \times 10^{12}$ Hz, while the velocity varies from 0 to $0.95c/n$ over a range $\Delta f \approx 3\kappa c/(2\pi n) = 3.7 \times 10^{12}$ Hz. In these expressions, the coupling constant [7]

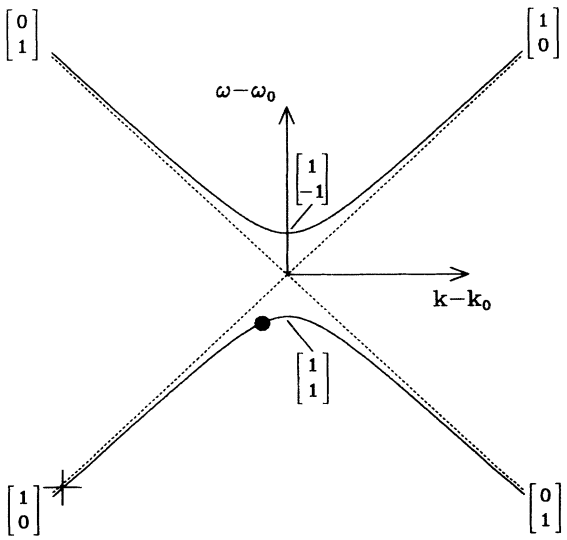

FIG. 1. Linear dispersion relation of a periodic medium (solid). The dotted line is the dispersion relation for a homogeneous medium with refractive index n. The column vectors show the different eigenvectors $\mathbf{v}_\pm$ for the Bloch functions of the periodic medium. The Bragg wave number $k_0 = \pi/d$ and ω_0 is the corresponding frequency.

$$\kappa = \frac{\pi \Delta n}{\lambda} \tag{1}$$

gives the strength of the coupling of forward- and backward-traveling modes. Over the same frequency range, the dispersion changes by a factor of 30. For radiation with $\lambda = 1.65\,\mu$m, the range Δf is only about 2% of the center frequency. Now by a nonlinear process, such as cross-phase modulation (XPM) [8,9], the frequency of a pulse may be shifted up or down the dispersion relation and so the pulse will experience a changing group velocity. This is exactly the case for a pulse-compression method, defined as the "optical pushbroom" effect in Ref. [10]. We use this effect below to illustrate our model.

The paper is structured as follows. In Sec. II we present a qualitative description of the optical pushroom. In Sec. III, we develop a model for the pushroom that takes into account the large change in dispersion seen by the pulse, deriving simple equations for the operation of the pushroom. We compare this model with exact numerical simulations in Sec. IV and present a discussion and conclusions in Sec. V.

II. OPTICAL PUSHBROOM —QUALITATIVE DESCRIPTION

The optical pushbroom (OPB) [10] is a proposed method of pulse compression in which a weak probe pulse is compressed in a grating by the influence of XPM from a copropagating strong pump pulse. The pump pulse is tuned far from the Bragg resonance and so propagates with a velocity $\alpha \approx c/n$. Moreover, it sees negligible dispersion and so for propagation through a grating of a few centimeters, its shape may be considered constant. Assuming the nonlinearity to be positive, the probe pulse is initially tuned at or near the lower band edge as indicated by the circle in Fig. 1 and is placed ahead of the pump. As the pump approaches the probe, by XPM, the leading edge of the pump induces a negative frequency shift on the trailing edge of the probe [8]. As the lower branch of the dispersion relation exhibits normal dispersion, the rear of the probe increases in velocity and begins to catch up with the leading edge producing pulse compression. With sufficient pump power, the frequency shift and consequent velocity increase is so rapid that the probe energy remains "piled up" on the front of the pump. As the probe compresses, the pump influences a greater proportion of the probe so that the whole pulse is compressed and swept out of the grating on the front of the pump. Central to the effect, is the shift in the probe frequency towards the asymptotic region of the dispersion relation where the dispersion vanishes and the group velocity approaches the speed of light, so that the probe may keep up with the pump. Hence, it is essential that a mathematical description of the OPB includes this asymptotic behavior. The operation of the OPB is illustrated in Fig. 2. The pump enters behind the probe in Fig. 2(a). After extended interaction with the pump, the probe is compressed and is carried to the right in Fig. 2(b). We discuss this figure in greater depth in Sec. IV.

The description of the OPB makes use of coupled-mode theory, by which nonlinear propagation in periodic media is governed by two coupled first-order partial differential equations [10] for the forward- and backward-traveling modes. It is known, however, that in the limit of low power and broad pulses, the general coupled-mode equations (CME) reduce to the NLSE [4]. This approach has proved useful in studying the properties of gap solitons, which in this approximation map onto the NLSE fundamental soliton. The extensive array of techniques that have been developed for studying the NLSE soliton, including the variational and moments approaches, for example [9,11–13], then have application to gap soliton studies. As we show below, by a similar argument the

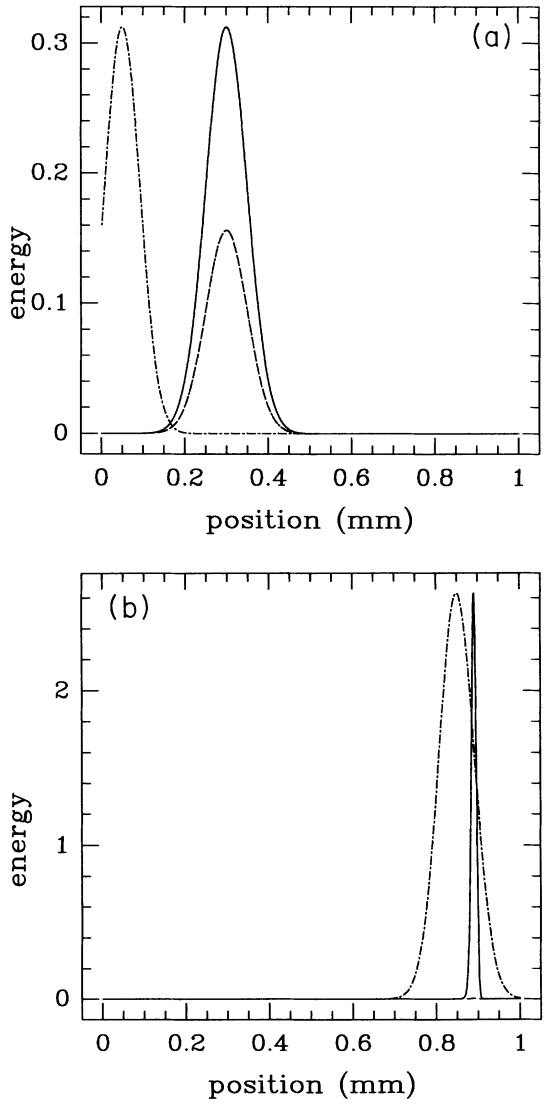

FIG. 2. (a) Energy density of fields at $t = 0$ in arbitrary units. Lines denote $|\mathcal{E}_+|^2$ (dotted), $|\mathcal{E}_-|^2$ (dashed), $|\mathcal{E}_+|^2 + |\mathcal{E}_-|^2$ (solid), Δ (dot-dashed). (b) As for (a) at $t = 8.4$ ps. The energy scales refer to the probe pulse. The pump has been scaled to fill the figures.

OPB equations may be reduced to a linear Schrödinger equation (LSE), but the presence of the frequency shift introduces an important complication.

III. THEORETICAL DESCRIPTION

A. Schrödinger equation description of grating structures

We now find a linear Schrödinger equation describing the propagation of the probe pulse through the grating. Our model is based on coupled-mode theory. We write the electric field in the grating as

$$\begin{aligned} E(x,t) = \{&[\mathcal{E}_p(x-\alpha t)\exp(-i\Omega_p t) \\ &+\mathcal{E}_+(x,t)]\exp(+ik_0 x) \\ &+\mathcal{E}_-(x,t)\exp(-ik_0 x)\}\exp(-i\omega_0 t) + \text{c.c.}, \end{aligned} \quad (2)$$

where c.c. denotes the complex conjugate and k_0 is the wave number corresponding to the Bragg frequency ω_0. Further, $\mathcal{E}_\pm$ are the slowly varying amplitudes of the forward- and backward-traveling modes comprising the weak probe, and $\mathcal{E}_p$ is the pump pulse amplitude with a detuning Ω_p from the Bragg frequency. Note that as discussed earlier, the pump sees a negligible dispersion so we further assume $\mathcal{E}_p$ to be a constant envelope traveling at the velocity α. We therefore consider it simply as a region of moving detuning or refractive index, rather than as a dynamical field. Inserting the ansatz (2) into the Maxwell wave equation, and using the slowly varying envelope approximation, the probe fields can be shown to satisfy [10]

$$\begin{aligned} &+i\frac{\partial \mathcal{E}_+}{\partial x} + i\frac{n}{c}\frac{\partial \mathcal{E}_+}{\partial t} + \kappa\mathcal{E}_- + \Delta(x,t)\mathcal{E}_+ = 0, \\ &-i\frac{\partial \mathcal{E}_-}{\partial x} + i\frac{n}{c}\frac{\partial \mathcal{E}_-}{\partial t} + \kappa\mathcal{E}_+ + \Delta(x,t)\mathcal{E}_- = 0, \end{aligned} \quad (3)$$

where

$$\Delta(x,t) = \Delta(x-\alpha t) = 2\Gamma|\mathcal{E}_p(x-\alpha t)|^2 \quad (4)$$

is the detuning of the probe from the grating due to cross-phase modulation with the pump, with Γ the nonlinear coupling coefficient. Note that as the pump Δ is completely determined, the system (3) is linear.

To find a NLSE corresponding to the system (3), we use the results of Ref. [4]. Writing $\mathcal{E}$ for the column vector $(\mathcal{E}_+, \mathcal{E}_-)$ and inserting the plane wave $\mathcal{E} = \mathbf{v}\exp[i(kx - \Omega t)]$ in Eqs. (3) in the absence of the pump [i.e., $\Delta(x,t) = 0$], leads to the solution

$$\Omega_\pm = \pm\frac{c}{n}\sqrt{\kappa^2 + k^2}, \quad (5)$$

with the corresponding (unnormalized) eigenvectors

$$\mathbf{v}_\pm = \begin{bmatrix} \kappa \\ k \mp \sqrt{\kappa^2 + k^2} \end{bmatrix}. \quad (6)$$

Thus in the linear limit, Eq. (5) gives rise to the dispersion relation in Fig. 1, while the vectors $\mathbf{v}_\pm$ are closely related to the Bloch functions of the medium on either branch of the dispersion relation, and indicate the relative strength of the forward and backward modes as a function of the wave number detuning k from the Bragg resonance [14]. Some values for the eigenvectors $\mathbf{v}$ of Eq. (6) are indicated in Fig. 1. Far from the resonance, the linear solutions are traveling plane waves represented by either the forward mode $\mathcal{E}_+$ or the backward mode $\mathcal{E}_-$, with the eigenvectors $(1,0)$ and $(0,1)$, respectively. At the band edges, the solutions are standing waves produced by an even (1,1) or odd combination (1,–1) of the two modes. In an idealized case of the pushbroom, the stationary probe would start out at the lower band edge with $\mathbf{v}_- = (1,1)$, an equal mixture of the forward and backward modes giving a zero total group velocity in a standing wave solution. After extended interaction with the pump, the probe frequency is shifted so far negatively that $\mathbf{v}_- \approx (1,0)$—all the probe energy is in the forward mode and the pulse moves at the speed of light in the medium.

The dispersion relation and eigenvectors completely describe the linear properties of the system. With the nonlinear effects introduced by cross-phase modulation, the properties of the system are naturally more complex and we use an approximate approach to proceed. We write the probe field in the form

$$\mathcal{E} = [a(x,t)\mathbf{v}_- + b(x,t)\mathbf{v}_+]\exp[i(kx - \Omega_- t)], \quad (7)$$

where the small correction term in $b(x,t)$ represents a "mixing" of the two Bloch functions by the pump [4]. Substituting this *ansatz* in Eqs. (3) and carrying out the procedure of Ref. [4], we find that b is completely determined by a, and for $\mathbf{v}_\pm$ normalized, is given by

$$b(\zeta,t) = \frac{i}{2}\frac{c}{n}\frac{\kappa}{(\kappa^2 + k^2)}\frac{\partial a}{\partial \zeta}. \quad (8)$$

Further, a satisfies the linear Schrödinger equation,

$$i\frac{\partial a}{\partial t} + \frac{1}{2}\Omega''_-\frac{\partial^2 a}{\partial \zeta^2} + \frac{c}{n}\Delta[\zeta - (\alpha - \Omega'_-)t]a(\zeta,t) = 0 \quad (9)$$

where the retarded distance is

$$\zeta = x - \Omega'_- t, \quad (10)$$

$(\alpha - \Omega'_-)$ is the relative velocity of the pump with respect to the probe and Δ may be thought of as a time-dependent potential moving at this relative velocity. Equations (8) and (9) describe the evolution of the probe pulse near the center frequency ω_p. As the probe frequency shifts lower, the "constants" Ω'_- and Ω''_- also evolve in a manner we determine later.

B. Moments approach

We can of course solve Eq. (9) numerically using the beam propagation method. However, approximate methods of solution can be both faster and more physically illuminating. To find a simple approximation of the prop-

agation at one frequency, we use a moments approach [12,13]. In this technique, the infinite dimensional system Eq. (9) is approximated by following the evolution of several lower order moments of the envelope function a. Here we choose the following three moments:

$$\begin{aligned} M_1 &= \int_{-\infty}^{\infty} \left|\frac{\partial a}{\partial \zeta}\right|^2 d\zeta, \\ M_2 &= \int_{-\infty}^{\infty} \zeta^2 |a|^2 \, d\zeta, \\ M_3 &= -i\int_{-\infty}^{\infty} \left(a^* \frac{\partial a}{\partial \zeta} - \frac{\partial a^*}{\partial \zeta} a\right) d\zeta, \end{aligned} \tag{11}$$

where the asterisk denotes the complex conjugate. We choose these three moments because they are the simplest that evolve in a lossless medium, and because in the absence of the nonlinearity, the first two lead to the exact results for dispersive spreading of a Gaussian pulse. The third moment is a measure of the pulse central frequency (or momentum).

Substituting Eqs. (11) in Eq. (9) and assuming that $|a|$ vanishes at large ζ, we find that the three moments evolve as

$$\begin{aligned} \frac{dM_1}{dt} &= i \int_{-\infty}^{\infty} \frac{\partial \Delta}{\partial \zeta}\left(\frac{\partial a^*}{\partial \zeta} a - a^* \frac{\partial a}{\partial \zeta}\right) d\zeta, \\ \frac{dM_2}{dt} &= \tfrac{i}{2}\Omega_-'' \int_{-\infty}^{\infty} \zeta^2 \left(a^* \frac{\partial^2 a}{\partial \zeta^2} - \frac{\partial^2 a^*}{\partial \zeta^2} a\right) d\zeta, \\ \frac{dM_3}{dt} &= 2 \int_{-\infty}^{\infty} \frac{\partial \Delta}{\partial \zeta} |a|^2 \, d\zeta. \end{aligned} \tag{12}$$

Equations (12) are still exact. Our approximation enters by assuming that the probe pulse can always be represented by the Gaussian form [8],

$$a = \frac{1}{\sqrt{\rho}} \exp\left(\frac{-\zeta^2}{2\rho^2}\right) \exp[i(\mu\zeta + \nu\zeta^2)], \tag{13}$$

and seek the evolution with t of the probe width ρ, center wave number μ, and linear wave number chirp ν. If we also take the pump to be Gaussian with fixed width σ:

$$\Delta(\zeta) = V_0^2 \exp\left(\frac{-\zeta^2}{\sigma^2}\right), \tag{14}$$

and substitute Eqs. (13) and (14) in Eqs. (11) and (12) we find the evolution equations

$$\frac{d\rho}{dt} = 2\Omega_-'' \rho\nu, \tag{15a}$$

$$\frac{d\nu}{dt} = \Omega_-''\left(\frac{1}{2\rho^4} - 2\nu^2\right) + \frac{V_0^2}{\sigma^2} h\left(\frac{2s^2}{\sigma^2+\rho^2} - 1\right), \tag{15b}$$

$$\frac{d\mu}{dt} = \frac{2V_0^2}{\sigma^2} hs, \tag{15c}$$

where

$$h = \left(\frac{\sigma^2}{\sigma^2+\rho^2}\right)^{\frac{3}{2}} \exp\left(-\frac{s^2}{\sigma^2+\rho^2}\right), \tag{16}$$

and the separation s between the centers of the pump and probe (defined such that s is negative if the probe leads the pump) is trivially given by

$$\frac{ds}{dt} = \alpha - \Omega_-' - \mu\Omega_-''. \tag{17}$$

We now briefly describe the nature of the system of Eqs. (15) and (16). Equation (15a), and the terms in Ω_-'' in Eq. (15b), give the exact result for dispersive spreading of a pulse in a uniform medium. The remaining terms in Eqs. (15b) and (15c) describe the effects of the pump. To understand their form we recall that the instantaneous wave number change induced on the probe is proportional to the gradient of the pump intensity [8], and thus the leading edge of the pump induces a negative wave number shift on the probe while the trailing edge induces a positive shift. Hence if the pump is behind the probe ($s < 0$), the probe is most strongly affected by the front of the pump and the average wave number μ becomes more negative, consistent with Eq. (15c). The dimensionless factor h describes the weakening of the shift as the separation of the pulses increases. Turning to the variation in wave number across the probe, the second term in Eq. (15b) describes the chirp induced on the probe because different portions of the probe are acted on by different parts of the pump. The chirp depends only on the absolute value of the pulse separation s, not on its sign: if the pulses are far apart $[2s^2/(\sigma^2+\rho^2) > 1]$, then the dominant effect is the interaction between the closest parts of each pulse. That is, the wave number shifts in the same direction across the whole pulse, but the shift is larger closer to the pump. The net effect is a positive chirp. When the two pulses are close, the wave number shifts in opposite directions on either side of the probe and the overall effect can be seen to be a negative chirp. Overall, the change in frequency and acceleration of the pulse during one period of propagation under Eq. (9) are given by the parameter μ. The compression of the pulse occurs through the chirp ν—if the frequency increases across the pulse, the rear will catch up to the front. We remark that similar calculations can be performed for pulse shapes other than Gaussian, but in general these do not yield results in terms of well-known functions [13].

C. Transformation of the probe frame

We now come to the key step of this section, in which we take account of the effects of the change in the probe frequency on the dispersion and group velocity of the pulse. The NLSE describes dispersion through a single constant coefficient

$$\Omega'' = \left.\frac{\partial^2 \Omega}{\partial k_0^2}\right|_{\Omega=\omega_p}, \tag{18}$$

where ω_p is the center frequency of the pulse, k_0 is the wave number, and $\Omega = \Omega(k_0)$ is the dispersion relation of the waveguide. The pulse group velocity

$$v_g = \Omega' = \left.\frac{\partial \Omega}{\partial k_0}\right|_{\Omega=\omega_p} \tag{19}$$

is thus fixed as a linear function of the pulse wave number. These quantities are also constants in our Eq. (9), expressing the fact that locally the dispersion relation is parabolic, although globally it is actually a hyperbola (see Fig. 1). In waveguides without gratings, the dispersion varies only slightly with frequency, and a global parabolic dispersion relation (constant Ω'') is often sufficient to model the medium. For pulses which are either very short (and hence have a broad frequency spectrum) or have a center frequency near the zero-dispersion point, the analysis can be improved by the addition of a cubic dispersion term [8]. As discussed in Sec. I, however, the constant dispersion approximation is most certainly not valid for the OPB, and so the moments analysis presented in Sec. III B does not alone correctly describe the pushbroom. In fact, Eq. (9) describes the probe momentarily, while the actual group velocity and dispersion are close to the constant values in the equation. After a short period of propagation under Eq. (9), the probe frequency and velocity change, and the coefficients Ω'_- and Ω''_-, are no longer suited to the pulse. Clearly, the coefficients must be adjusted during the propagation to match the changing velocity of the frame in which the probe is at rest. Recalling that the NLSE is usually written in a frame moving with the pulse group velocity as is true for Eq. (9), our approach is seen to generalize this, by recognizing that the velocity of the comoving frame changes during propagation due to the influence of the pump pulse.

To accomplish the change of frame, we need to rewrite the field (7) in the form

$$\hat{\mathcal{E}} = (\hat{a}\hat{\mathbf{v}}_- + \hat{b}\hat{\mathbf{v}}_+)\exp[i(\hat{k}s - \hat{\Omega}_- t)], \tag{20}$$

where the caret indicates the corresponding quantity in the new frame. We are free to move to any sensible frame, the most obvious being that in which the wave number μ becomes zero. For the procedure to be valid, we must demand that $\hat{b}$ satisfies a relation of the form of Eq. (8) in terms of the new variables. Given the choice of new frame, a unique set of transformations can be found, for which to first order,

$$\hat{a} = a\exp(-i\mu x), \tag{21}$$

$$\hat{b} = b - i\mu a, \tag{22}$$

$$\hat{k} = k + \mu, \tag{23}$$

$$\hat{\Omega}_- = \Omega_- + \mu\Omega'_-. \tag{24}$$

Thus the parameter k measures the wave number of the point on the dispersion relation corresponding to the most recent change of frame, while μ is the wave-number shift from that point while the pulse travels in that frame. In this procedure, we neglect smaller terms in $\hat{b}$. We can now find the new values of Ω'_- and Ω''_- from Eq. (5) and continue propagation with Eqs. (15) and (17) repeating the change of frame at regular intervals in a steplike fashion. Equation (22) gives us a criterion for the minimum frequency with which the frame should be changed—the product μa should at most be comparable in size to b.

As well as this steplike approach we can present the problem in a continuous manner: Increasing the frequency of changes of frame without bound, we reach the limit in which the group velocity and dispersion coefficients are adjusted constantly, and at all times the NLSE is written in the frame of the instantaneous velocity of the probe. We can cast Eqs. (15) to reflect this approach, by writing $\Omega'_-(k)$ and $\Omega''_-(k)$ explicity as functions of k and using Eq. (15c) to measure the change in total wave number k rather than the "local wave number" μ which is identically zero because the NLSE is always in exactly the frame of the probe. For the same reason, the final term in Eq. (17) vanishes and may be dropped. While the continuous approach may appear more aesthetic, we emphasize that provided the criterion $b \ll \mu a$ is satisfied, the stepwise and continous approaches are equally valid within the approximations of the model.

Equations (21) and (24) are notable in showing that although the nature of the Bloch functions changes from standing waves at the band edge, to plane waves far from the gap [see the discussion following Eq. (6)], the envelope function $a(\zeta)$ changes only in phase under a change of frame. While for a homogeneous medium, one might expect that simply making Ω'_- and Ω''_- functions of k would be sufficient to incorporate strongly varying dispersion, it is perhaps surprising that the same is true in a grating structure.

IV. NUMERICAL EXAMPLES

We now compare the predictions of our model with exact numerical simulations of Eqs. (3). The simulations are performed using a fourth-order collocation technique described in Ref. [15]. The predictions of the model are found by integrating Eqs. (15)–(17) using a fourth-order Runge-Kutta algorithm with the change of frame given by Eqs. (21)–(24) performed sufficiently often to satisfy the criterion $b \ll \mu a$. The simulations presented here model a GaAs-$Al_xGa_{1-x}As$ grating with an average refractive index of $n = 3.14$ and an index modulation of $\Delta n = 0.042$. For illumination at $\lambda = 1.65\,\mu$m, and a grating length of $L = 1$ mm, this gives a grating strength of $\kappa L = 80$. In addition, we assume a nonlinearity of $n^{(2)} = 2 \times 10^{-17}\,\mathrm{m}^2/\mathrm{W}$, and a pump peak power of 10.2 kW. For a focal spot of circular cross section with radius 2 μm and effective area 12.6 $\mu\mathrm{m}^2$, the pump will produce a maximum index change of $\Delta n_{\mathrm{NL}} = 0.016$. Figure 2 demonstrates the operation of the pulse compression for this geometry with pump width $\sigma = 60\,\mu$m, initial probe width $\rho = 70$ μm, initial pulse separation $s = 250\,\mu$m, and pump velocity $\alpha = c/n$. Figure 2(a) shows this starting configuration. The pump intensity is represented by the dot-dashed line, the forward probe intensity $|\mathcal{E}_+|^2$ by the dotted line, the backward probe intensity $|\mathcal{E}_-|^2$ by the dashed line, and the total probe intensity by the solid line. At $t = 0$, the probe has zero velocity and equal energy in the forward and backward modes. At $t = 8.4$ ps, shown in Fig. 2(b) as the pump leaves the grating, the probe has been swept to the right by the pump and significantly compressed, the peak intensity having increased

by a factor of over 8. The backward (dashed) mode now contains only a tiny fraction of the total probe energy, indicating the change in frequency and shift away from the Bragg resonance.

Figure 3(a) shows the peak position of the probe pulse for this case, according to our model (solid), the simulator (dashed) and the moments approach in which the LSE with constant coefficients is used (dotted). For this latter curve, the dispersion is assumed to have a constant value equal to half the value of the dispersion at the band edge—chosen as a reasonable average measure of the dispersion. We note that the predictions of this approach are not significantly improved by choosing different constant values. Figure 3(b) shows predictions of the width ρ by the same three methods. For pulses which are not exactly Gaussian, there is a degree of arbitrariness in the choice of a measure of width. For the numerical simulations, we find the width ρ by measuring the full width at half maximum (FWHM) and dividing by the Gaussian conversion factor $2\sqrt{\ln 2}$. The present model is in good quantitative agreement with the numerical simulation, and in particular predicts the correct asymptotic behavior while the constant coefficient model does not. The inclusion of frequency shifting is thus clearly essential here as discussed in Sec. II.

The initial peak in the width which is not predicted by either analytic model is due to the non-Gaussian form of the exact result. In fact, simulations reveal that when the pulses first begin to overlap and interact, the probe becomes asymmetric and the peak briefly moves backwards towards the pump. This effect is visible around $t = 1.5$ ps in Fig. 3(a). In light of this, we have also compared the model width with a "second-moment" width $\bar{\rho}$ calculated from the simulator results with the definition

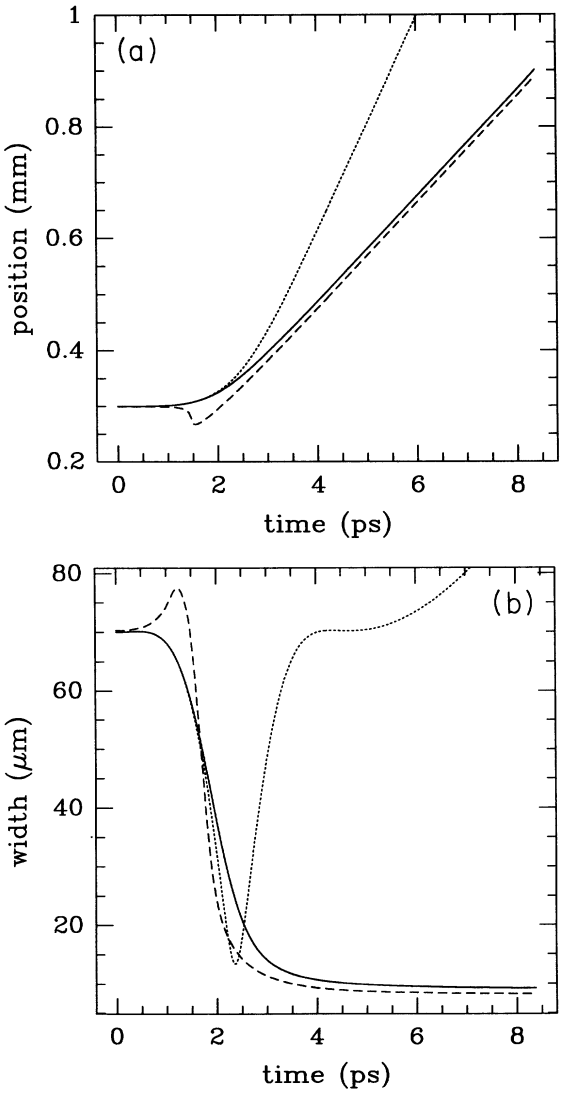

FIG. 3. (a) Position of the peak of the probe pulse for the simulation of Fig. 2 and (b) width of the probe pulse, according to our model (solid), the exact simulation (dashed) and the NLSE without change of frame (dotted).

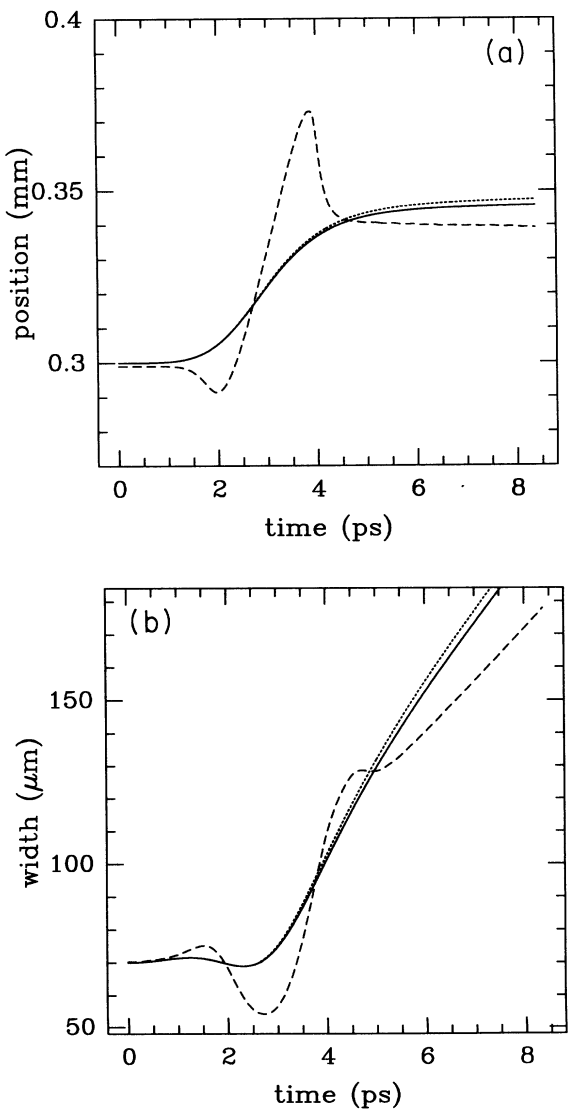

FIG. 4. (a) Position and (b) width of the probe for a case with a peak pump power of 1.9 kW. Line styles are as in Fig. 3.

$$\bar{\rho} = \left(\frac{\int_{-\infty}^{\infty} |a|^2 (\zeta - \zeta_0)^2 \, d\zeta}{\int_{-\infty}^{\infty} |a|^2 \, d\zeta} \right)^{1/2}, \tag{25}$$

where ζ_0 is the mean position of the energy in the pulse. This measure is weighted by the distribution of energy in the pulse and is less prone to brief fluctuations than the FWHM. The model predictions are found to agree even more closely with this measure $\bar{\rho}$ than with the FWHM. Note that for exactly Gaussian pulses, the two definitions are trivially related by $\rho = \sqrt{2}\bar{\rho}$.

In Fig. 4 we show the results for a case with parameters identical to those of Fig. 3 except that the pump peak power is reduced to 1.9 kW. In this case, the frequency shift induced on the probe is insufficient to allow it to keep up with the pump. Although the plot of position shows an initial slight acceleration, the pump still catches up easily. From the moment when the center of the pump overtakes the center of the probe, the probe is most strongly affected by the trailing edge of the pump. It thus experiences a net positive frequency shift back towards the band edge with a corresponding deceleration. The overall effect is that the probe is shifted to the right by about 0.05 mm and then left behind with a negligible velocity. Similarly, Fig. 4(b) shows that although the probe is initially compressed by a weak pushbroom action, dispersive spreading dominates once the pump has walked through the probe. As the frequency shift in this case is relatively small and short-lived, the inclusion of frequency shifting has little effect on the predictions—the dispersion may be successfully modeled as a constant.

V. DISCUSSION AND CONCLUSION

While we have demonstrated the applicability of our simple model, the simulations imply that the pushbroom effect for a pulsed probe can only be observed in this geometry at high pump intensities, above 10^9 W/cm^2. We note in passing though, that for a cw probe tuned to a transmission resonance of the grating, the effect should occur at substantially lower powers [10]. We now consider two possible techniques which could be thought likely to reduce the pump power needed for effective action of the optical pulse compression. Clearly, for significant effects to occur, the pulse frequency must change by an amount of the order of $\kappa c/n$—the scale on which the velocity and dispersion vary. It would seem then, that the effect should appear at lower pump powers in weak gratings where κ is small and the necessary frequency shift is reduced. With weaker gratings, however, the forward and backward modes in the initial probe pulse are weakly coupled and move apart rapidly. This is shown explicitly by the relation which holds at the lower band edge

$$\Omega_-'' = -\frac{c}{n\kappa}. \tag{26}$$

Thus, the envelope function $a(\zeta, t)$ which describes both the modes, initially experiences stronger dispersion in weak gratings and in the absence of the pump, broadens more rapidly. To overcome this broadening, broader optical pulses and longer gratings are required—the power requirement can only be reduced at the expense of longer geometries. In optical fibers, for example, the gratings are somewhat weaker and the change in velocity can occur in under 0.1% of the optical frequency, while the gratings are indeed much longer than in semiconductor structures—typically a centimeter. The glass nonlinearity, however, is three orders of magnitude less than in GaAs, so that the power requirements remain severe. We remark also that Eq. (26) is at first somewhat surprising—the dispersion due to the grating increases without bound as the grating strength vanishes. Mathematically, this limit is due to the dispersion relation becoming increasingly nonparabolic at the band edge, as the grating strength decreases. To see the physical consequence of this, we recall that the envelope function $a(\zeta, t)$ represents a pulse comprised of two modes traveling in opposite directions. In a strong grating, energy is continually coupled between the modes and the pulse remains well confined for some time. In the limit of a vanishing grating, the pulse splits into two pulses, one in each mode, which separate at the speed of light with virtually no mutual interaction. The envelope function a approximates this behavior by broadening very rapidly under the influence of the very large dispersion Ω_-''.

We remarked before that the shift in instantaneous probe frequency is proportional to the gradient of the intensity of the pump pulse [8]. Hence, at first sight, it seems that the frequency shift may be maintained if a reduction in the pump power is accompanied by a decrease in the pump width, so as to keep the pump intensity gradient constant. Numerical simulations reveal that while this is true to an extent, the details are not straightforward. Reducing the pump width also reduces the available interaction time between the pump and probe in which the probe may be accelerated. This typically leads to situations in which a large component of the probe energy is not compressed but falls behind the pump, with a small fraction of the energy remaining on the pump. Such a case is shown in Fig. 5. This simulation has the same parameters as for Fig. 2 except that the pump width is reduced by a factor 3 and the intensity by a factor 0.5. The pump intensity gradient is thus greater than for Fig. 2 and yet the pushbroom action is far less effective. In other similar simulations we have observed the formation of multiple peaks in the probe. In such cases, when the probe shape is highly non-Gaussian, our model is naturally far less successful. For the simulation of Fig. 5 both the frequency shifting and non-shifting approaches predict that the pump walks through the probe as in Fig. 4. In general, our model should be less successful as the pump width decreases. The model assumes that the chirp on the probe is linear which is a reasonable approximation if the probe sees only a small fraction of the pump pulse at any particular time. If the pump is narrow, then the actual chirp imposed on the probe is more complicated and the model will begin to fail.

As many high-powered lasers produce soliton pulses, it would be useful to model the OPB when the pulses were assumed to have hyperbolic secant shapes rather

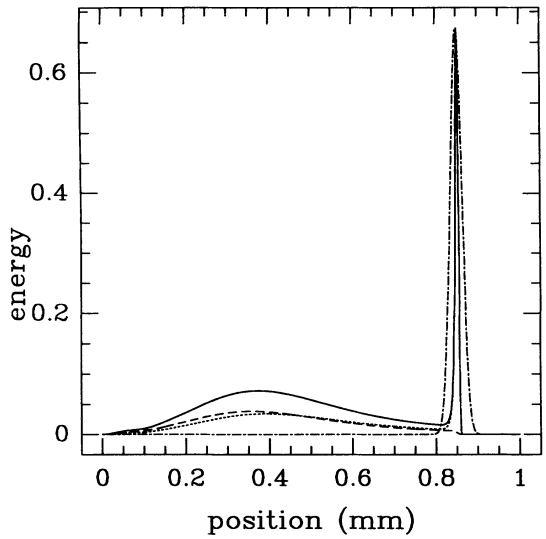

FIG. 5. Pump and probe energies in arbitrary units at $t = 8.4$ ps. Parameters are as for Fig. 3 with pump width reduced to $\sigma = 20$ μm and pump intensity reduced to 5.2 kW.

than Gaussians. Unfortunately, if either or both fields have sech shapes, the integrals (12) do not in general exist. One approach to gaining some analytic insight is to choose Gaussian pulses which have the same energy and second moment width as the input sech pulses.

A significant addition still required, is to model the pump as a fully dynamical field rather than as an inert moving detuning, allowing self-phase modulation to act on the pump, and permitting the exchange of energy between the two pulses. An extension of the moments method that preserved the total energy in the grating, but not the energies of the individual pulses would be one possibility for incorporating these effects.

In conclusion, we have developed a simple model that describes the optical pushbroom by a Schrödinger-type equation modified to take account of the large frequency shifts induced on the probe. We have demonstrated the importance of including the frequency change when the pump intensity is large enough for the pulse compression action to occur. Reduction in the necessary pump power will be most easily achieved by using long weak grating structures.

ACKNOWLEDGMENTS

M.J.S. thanks Dr. Leon Poladian of the OFTC for many helpful discussions. M.J.S. is grateful for the financial support from APRA and ATERB. This work was supported in part by the Optical Fibre Technology Centre, which is a partner in the Australian Photonics Cooperative Research Centre.

[1] L. F. Mollenauer, R. H. Stolen, and J. P. Gordon, Phys. Rev. Lett. **45**, 1095 (1980).
[2] J. E. Rothenberg, Opt. Lett. **15**, 495 (1990).
[3] J. E. Sipe and H. G. Winful, Opt. Lett. **13**, 132 (1988).
[4] C. M. de Sterke and J. E. Sipe, Phys. Rev. A **42**, 550 (1990).
[5] S. T. Ho *et al.*, Appl. Phys. Lett. **59**, 2558 (1991).
[6] G. Meltz, W. W. Morey, and W. H. Glenn, Opt. Lett. **14**, 823 (1989).
[7] H. Kogelnik and C. V. Shank, J. Appl. Phys. **43**, 2327 (1972).
[8] G. P. Agrawal, *Nonlinear Fiber Optics* (Academic Press, San Diego, CA, 1989).
[9] B. Jaskorzynska and D. Schadt, IEEE J. Quant. Electron. **24**, 2117 (1988).
[10] C. M. de Sterke, Opt. Lett. **17**, 914 (1992).
[11] D. Anderson, Phys. Rev. A **27**, 3135 (1983).
[12] E. Caglioti, B. Crosignani, and P. Di Porto, Phys. Rev. A **38**, 4036 (1988).
[13] T. Ueda and W. L. Kath, Phys. Rev. A **42**, 563 (1990).
[14] C. M. de Sterke and J. E. Sipe, Prog. Opt. (to be published).
[15] C. M. de Sterke, K. R. Jackson, and B. D. Robert, J. Opt. Soc. Am. B **8**, 403 (1991).